JAIST Repository
https://dspace.jaist.ac.jp/

Title	Low-frequency noise in AlN/AlGaN/GaN metal-insulator-semiconductor devices: a comparison with Schottky devices
Author(s)	Le, Son Phuong; Nguyen, Tuan Quy; Shih, Hong-An; Kudo, Masahiro; Suzuki, Toshi-kazu
Citation	Journal of Applied Physics, 116(5): 54510-1-54510-8
Issue Date	2014-08-07
Type	Journal Article
Text version	publisher
URL	http://hdl.handle.net/10119/12903
Rights	Copyright 2014 American Institute of Physics. This article may be downloaded for personal use only. Any other use requires prior permission of the author and the American Institute of Physics. The following article appeared in Son Phuong Le, Tuan Quy Nguyen, Hong-An Shih, Masahiro Kudo, and Toshi-kazu Suzuki, Journal of Applied Physics, 116(5), 54510- (2014) and may be found at http://dx.doi.org/10.1063/1.4892486
Description	

JAIST
JAPAN
ADVANCED INSTITUTE OF
SCIENCE AND TECHNOLOGY

Japan Advanced Institute of Science and Technology

JOURNAL OF APPLIED PHYSICS 116, 054510 (2014)

Low-frequency noise in AlN/AlGaN/GaN metal-insulator-semiconductor devices: A comparison with Schottky devices

Son Phuong Le, Tuan Quy Nguyen, Hong-An Shih, Masahiro Kudo, and Toshi-kazu Suzuki[a)]

Center for Nano Materials and Technology, Japan Advanced Institute of Science and Technology (JAIST), 1-1 Asahidai, Nomi, Ishikawa 923-1292, Japan

(Received 3 June 2014; accepted 27 July 2014; published online 7 August 2014)

We have systematically investigated low-frequency noise (LFN) in AlN/AlGaN/GaN metal-insulator-semiconductor (MIS) devices, where the AlN gate insulator layer was sputtering-deposited on the AlGaN surface, in comparison with LFN in AlGaN/GaN Schottky devices. By measuring LFN in ungated two-terminal devices and heterojunction field-effect transistors (HFETs), we extracted LFN characteristics in the intrinsic gated region of the HFETs. Although there is a bias regime of the Schottky-HFETs in which LFN is dominated by the gate leakage current, LFN in the MIS-HFETs is always dominated by only the channel current. Analyzing the channel-current-dominated LFN, we obtained Hooge parameters α for the gated region as a function of the sheet electron concentration n_s under the gate. In a regime of small n_s, both the MIS- and Schottky-HFETs exhibit $\alpha \propto n_s^{-1}$. On the other hand, in a middle n_s regime of the MIS-HFETs, α decreases rapidly like $n_s^{-\xi}$ with $\xi \sim$ 2-3, which is not observed for the Schottky-HFETs. In addition, we observe strong increase in $\alpha \propto n_s^3$ in a large n_s regime for both the MIS- and Schottky-HFETs. © *2014 AIP Publishing LLC*. [http://dx.doi.org/10.1063/1.4892486]

I. INTRODUCTION

GaN-based metal-insulator-semiconductor heterojunction field-effect transistors (MIS-HFETs) have been extensively developed as devices for high-frequency and high-power applications, owing to the merits of gate leakage reduction and passivation effects. As a gate insulator, high-dielectric-constant (high-*k*) oxides such as Al_2O_3,[1] HfO_2,[2,3] or ZnO,[4] and high-*k* nitrides having high thermal conductivities such as AlN[5–8] or BN,[9,10] were employed. In the GaN-based MIS-HFETs, low-frequency noise (LFN) will be strongly influenced by the insulator itself and/or the insulator-semiconductor interface, and also by the gate leakage reduction. Although LFN in the GaN-based devices has been studied for a long time, the previous studies mainly focused on Schottky-HFETs[11–29] and MIS-HFETs with oxide gate insulators[4,30–38] with a few exception of a SiN gate insulator.[39] Moreover, in LFN studies for FETs, it is often difficult to identify the contributions from the intrinsic gated and extrinsic ungated parts. Therefore, it is important to obtain insights of LFN in GaN-based MIS-HFETs with nitride insulators such as AlN, comparing with Schottky-HFETs and clarifying the contributions from the intrinsic and extrinsic parts.

In this work, in order to elucidate LFN in AlN/AlGaN/GaN MIS-HFETs comparing with that in AlGaN/GaN Schottky-HFETs, we systematically characterized both ungated two-terminal devices and the HFETs. From the characterization, LFN behavior in the intrinsic gated region was extracted for the MIS- and Schottky-HFETs. Although there is a bias regime of the Schottky HFETs in which LFN is dominated by the gate leakage current, LFN in the MIS-HFETs is always dominated by only the channel current. Analyzing the channel-current-dominated LFN, we obtain Hooge parameters α for the gated region as a function of the sheet electron concentration under the gate, which exhibits different behaviors for the MIS- and Schottky-HFETs.

II. DEVICE FABRICATION

Using $Al_{0.27}Ga_{0.73}N$(30 nm)/GaN(3000 nm) heterostructure obtained by metal-organic vapor phase epitaxy on sapphire (0001), we fabricated AlN/AlGaN/GaN MIS devices, i.e., HFETs as well as ungated two-terminal devices. The same sets of AlGaN/GaN Schottky devices, i.e., HFETs and ungated two-terminal devices, were fabricated simultaneously. The fabrication process is as follows.[7,8] On the AlGaN/GaN heterostructure, Ti/Al/Ti/Au Ohmic electrodes were formed and device isolation was achieved by B^+ ion implantation. For MIS devices, a 20-nm-thick AlN film as a gate insulator was deposited on the AlGaN surface by RF magnetron sputtering at room temperature with an AlN target in Ar-N_2 ambient, following the surface treatments, which include oxygen plasma ashing and cleaning by the organic solvents (for removing organic contaminants), and cleaning by Semicoclean (for removing oxides). The formation of Ni/Au gate electrodes on AlN (MIS-HFETs) or AlGaN (Schottky-HFETs) completed the device fabrication process. The HFETs have gate length $L_G = 260$ nm, the source-gate spacing of 2 μm, the gate-drain spacing of 3 μm, and the gate width $W = 50$ μm. The ungated two-terminal devices have the width $W = 50$, 100 μm and electrode spacing of $L =$ 2-16 μm. Schematics of the devices are shown in Fig. 1.

[a)]Author to whom correspondence should be addressed. Electronic mail: tosikazu@jaist.ac.jp

 © 2014 AIP Publishing LLC

[This article is copyrighted as indicated in the article. Reuse of AIP content is subject to the terms at: http://scitation.aip.org/termsconditions. Downloaded to] IP: 150.65.7.11 On: Mon, 14 Sep 2015 04:02:23

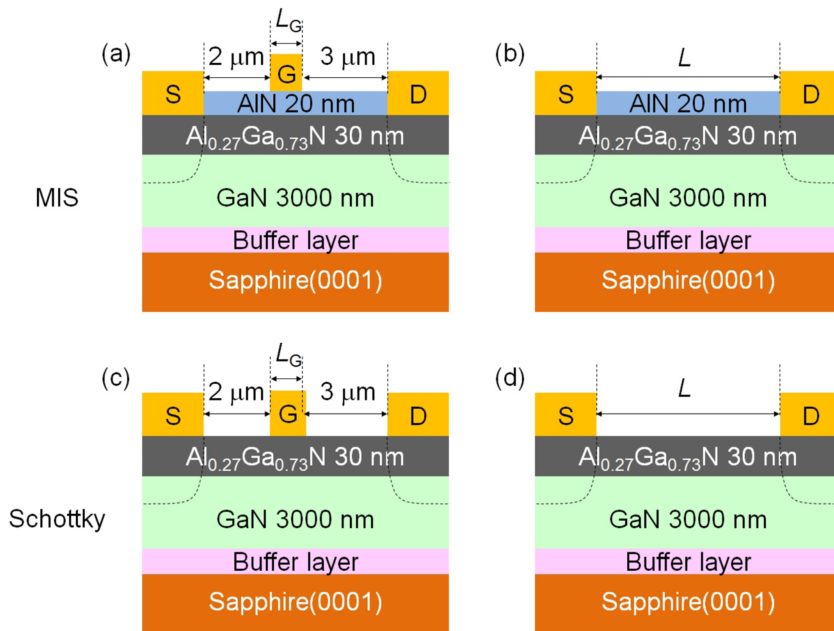

FIG. 1. Schematics of (a) MIS-HFET, (b) MIS ungated two-terminal device, (c) Schottky-HFET, and (d) Schottky ungated two-terminal devices.

III. DC CHARACTERIZATION OF DEVICES

DC characterization was carried out for the ungated two-terminal devices and the HFETs. From the transfer length method or transmission-line model (TLM) measurements of the ungated devices, we obtain a contact resistance $r_c = 2.4\,\Omega\,\text{mm}$, and two-dimensional electron gas (2DEG) sheet resistances of the ungated region $r_{sug} = 790$ and $450\,\Omega$/sq. for the MIS and Schottky ungated devices, respectively. Hall-effect measurements show the electron mobility of 1200 and $1500\,\text{cm}^2$/V-s, and sheet electron concentration of $n_{sug} = 6.4 \times 10^{12}$ and $9.3 \times 10^{12}\,\text{cm}^{-2}$, for the MIS and Schottky ungated devices, respectively. Figures 2(a) and 2(b) show output characteristics (normalized by the gate width W) of the MIS- and Schottky-HFETs, respectively, where I_D is the drain current. (Considering LFN characterization, throughout this article, we employ the definition of currents in the unit of [A] without normalization by the device width; the vertical axis of Fig. 2 shows I_D/W in the unit of [mA/mm].) The Schottky-HFET exhibits negative drain current for large forward gate-source voltages V_G and small drain-source voltages V_D, owing to large gate leakage currents. Transfer characteristics (normalized by the gate width W) is shown in Fig. 3, where I_G is the gate current and g_m is the transconductance: (a) and (b) for the MIS-HFETs, (c) and (d) for the Schottky-HFETs, (a) and (c) for $V_D = 10\,\text{V}$ in the saturation regime, and (b) and (d) for $V_D = 0.1$ V in the linear regime. For the MIS-HFETs, gate currents are significantly small, 10^{-9} A/mm range or less, about 4 orders for reverse and 8 orders for forward gate biases smaller than those of the Schottky-HFETs, owing to good insulating properties of the AlN. The small gate leakage currents lead to small drain off-currents shown in Figs. 3(a) and 3(b).

IV. LFN CHARACTERIZATION OF DEVICES

For LFN characterization of the devices, we employed a measurement system consisting of a shielded probe station, a low-noise pre-amplifier (LNA, Stanford SR570), and a dynamic signal analyzer (DSA, Agilent 35670 A). To measure the ungated two-terminal devices, inside the shielding chamber of the probe station, one Ohmic electrode of the device is

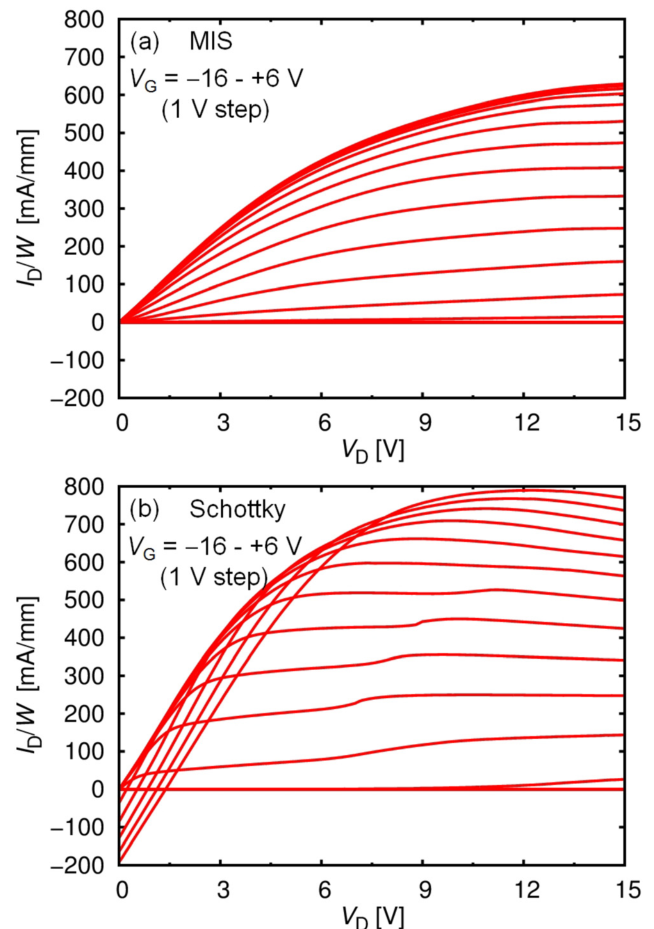

FIG. 2. Output characteristics of (a) MIS- and (b) Schottky-HFETs. Drain current I_D normalized by the gate width W as a function of drain-source voltage V_D is obtained by changing gate-source voltage V_G.

[This article is copyrighted as indicated in the article. Reuse of AIP content is subject to the terms at: http://scitation.aip.org/termsconditions. Downloaded to] IP: 150.65.7.11 On: Mon, 14 Sep 2015 04:02:23

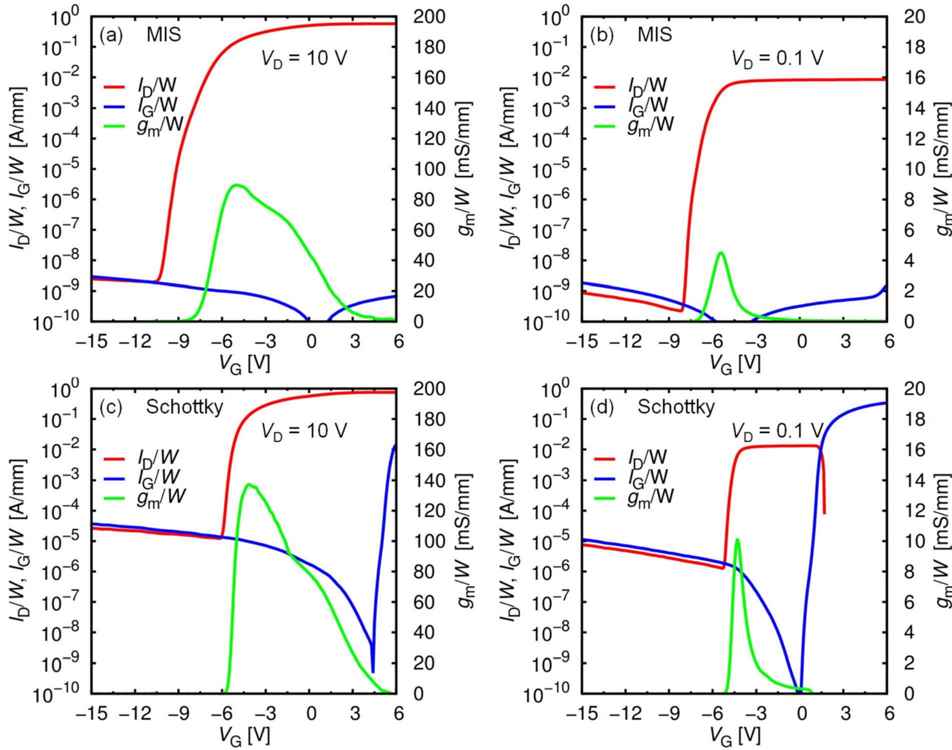

FIG. 3. Transfer characteristics with gate current I_G and transconductance g_m: (a) and (b) for MIS-HFETs, (c) and (d) for Schottky-HFETs, (a) and (c) for $V_D = 10$ V in the saturation regime, and (b) and (d) for $V_D = 0.1$ V in the linear regime.

connected to the LNA with applications of a DC bias voltage and a DC offset current, while the other Ohmic electrode is grounded. The current noise is amplified by the LNA, whose output is entered to the DSA to obtain the power spectrum density (PSD). For measurements of the HFETs, inside the shielding chamber, the source is grounded, the drain is connected to the LNA with applications of a DC bias drain voltage and a DC offset drain current, and a gate voltage is applied from a parameter analyzer through an *RC* passive low-pass filter (LPF) with a cut-off frequency ∼0.05 Hz to eliminate the noise from the parameter analyzer. According to specification of the LPF and the DSA, we obtain the current noise PSD for a frequency range of $f = 1\text{-}10^4$ Hz.

We first measured LFN in the ungated two-terminal devices. Figures 4(a) and 4(b) show examples of measurement results of current noise PSD S_I for the Ohmic regime of the MIS and Schottky ungated devices, respectively, with $W = 100\,\mu$m and $L = 2$, $16\,\mu$m. We observe $1/f$ behavior satisfying $S_I/I^2 \simeq K/f$, with a constant factor K depending on the device size, where the DC current I is varied by changing the bias voltage V. No specific bump suggests no specific high-density electron traps with a specific time constant. In order to evaluate the factor K, we plot $S_I f$ as functions of I in Figs. 5(a) and 5(b) for the MIS and Schottky ungated devices, respectively, where we can confirm $S_I f \propto I^2$.

Since the total resistance of the two-terminal ungated devices is given by $R = 2R_c + R_{2DEG}$, where $R_c = r_c/W$ from the contact and $R_{2DEG} = r_{sug}\, L/W$ from the ungated 2DEG, we obtain S_I of the series-connected resistance

$$S_I = S_I^{c} \frac{2{R_c}^2}{(2R_c + R_{2DEG})^2} + S_I^{2DEG} \frac{{R_{2DEG}}^2}{(2R_c + R_{2DEG})^2}, \qquad (1)$$

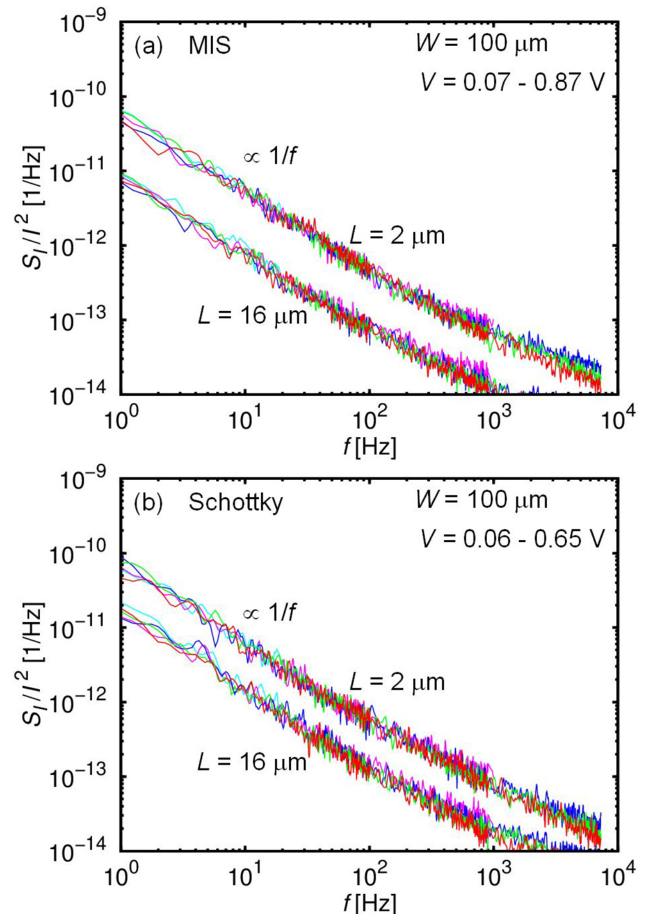

FIG. 4. S_I/I^2 as functions of f for (a) MIS and (b) Schottky ungated two-terminal devices.

[This article is copyrighted as indicated in the article. Reuse of AIP content is subject to the terms at: http://scitation.aip.org/termsconditions. Downloaded to] IP: 150.65.7.11 On: Mon, 14 Sep 2015 04:02:23

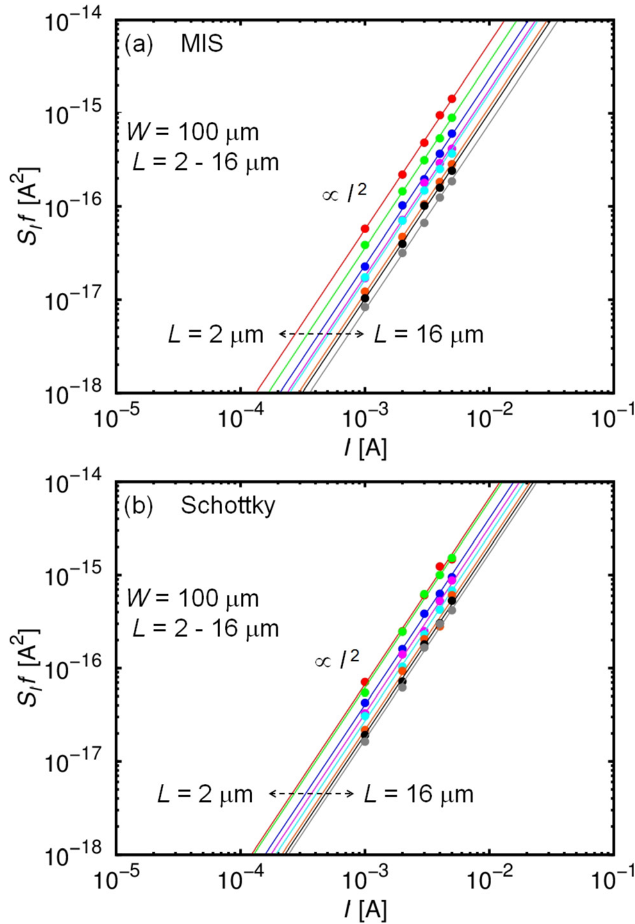

FIG. 5. $S_I f$ as functions of I for (a) MIS and (b) Schottky ungated two-terminal devices.

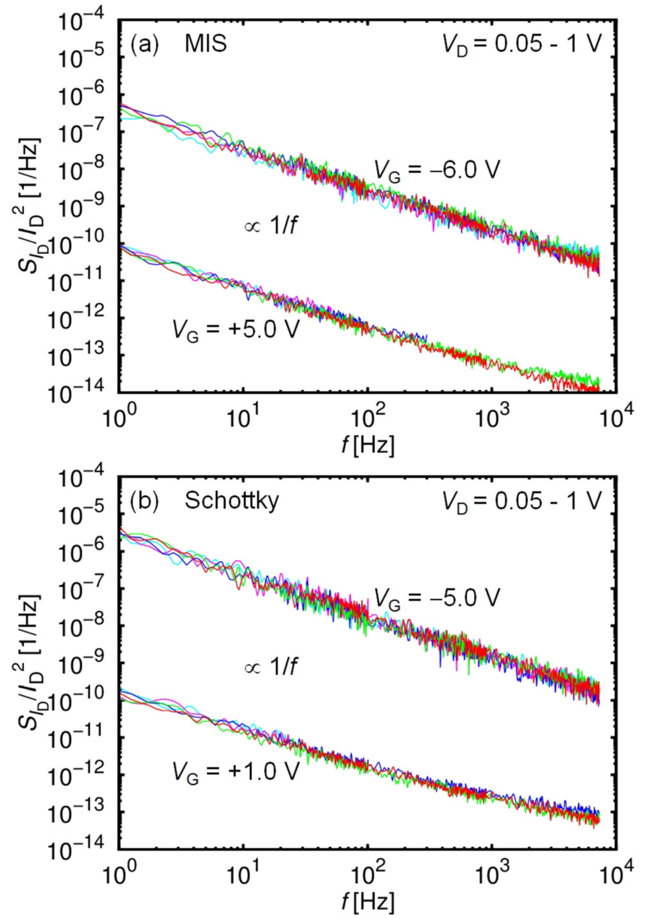

FIG. 7. $S_{I_D}/I_D{}^2$ as functions of f for (a) MIS- and (b) Schottky-HFETs.

where S_I^{c} and S_I^{2DEG} are the current noise PSD generated by one contact and the ungated 2DEG, respectively. Hence, we obtain

$$K = \frac{S_I f}{I^2} = K_c \frac{2R_c{}^2}{(2R_c + R_{2DEG})^2} + K_{2DEG} \frac{R_{2DEG}{}^2}{(2R_c + R_{2DEG})^2}, \quad (2)$$

where K_c and K_{2DEG} are the factors for one contact and the ungated 2DEG, respectively. The latter is obtained by the Hooge theory[40]

$$K_{2DEG} = \frac{\alpha_{ug}}{N} = \frac{\alpha_{ug}}{n_{sug} LW}, \quad (3)$$

where α_{ug} is the Hooge parameter and N is the total electron number of the ungated 2DEG. Since $R_c \propto 1/W$, $R_{2DEG} \propto L/W$, $K_c \propto 1/W$, and $K_{2DEG} \propto 1/LW$, KW is a single-valued function of the electrode spacing L as shown in Fig. 6(a) with the fitting line. Using the relation $RW = 2r_c + r_{sug}L$, we also obtain KW as a single-valued function of RW as shown in Fig. 6(b) with the fitting line. From the fitting, we can evaluate $K_c W \simeq 1.9 \times 10^{-12}$ cm, which is common for the MIS and Schottky devices because of the same Ohmic process. We also obtain $\alpha_{ug} \simeq 2.2 \times 10^{-4}$ and

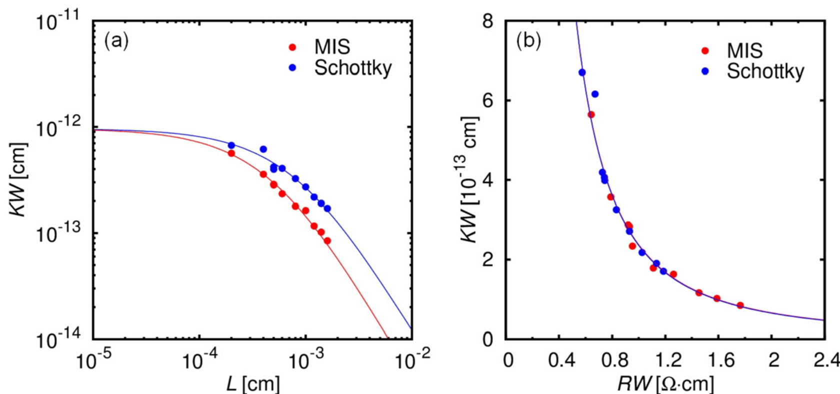

FIG. 6. (a) KW as a function of the electrode spacing L and (b) as a function of RW for MIS and Schottky ungated two-terminal devices.

[This article is copyrighted as indicated in the article. Reuse of AIP content is subject to the terms at: http://scitation.aip.org/termsconditions. Downloaded to] IP: 150.65.7.11 On: Mon, 14 Sep 2015 04:02:23

5.0×10^{-4} for the ungated region of the MIS and Schottky devices, respectively. The smaller Hooge parameter α_{ug} in the MIS devices can be attributed to the lower electron mobility due to additional scattering mechanisms caused by the gate insulator deposition, where the mobility fluctuation dominates α_{ug} according to the Hooge theory.[40]

We next measured LFN in the HFETs. Figures 7(a) and 7(b) show examples of measurement results of drain current noise PSD S_{I_D} for the linear regime of the MIS- and Schottky-HFETs, respectively, with the fixed gate voltages V_G. We also observe $1/f$ behavior satisfying $S_{I_D}/I_D{}^2 \simeq K_{HFET}/f$ with a factor K_{HFET} depending on the fixed V_G, where the drain current I_D is varied by changing the drain voltage V_D. For the purpose of the evaluation of the factor K_{HFET}, in Figs. 8(a) and 8(b), we plot $S_{I_D}f$ as functions of I_D for the MIS- and Schottky-HFETs, respectively, where we can confirm $S_{I_D}f \propto I_D{}^2$. The factor K_{HFET} for the MIS- and Schottky-HFETs as a function of V_G is plotted in Figs. 9(a) and 9(b), respectively, where the drain current I_D and the gate current I_G for $V_D = 0.1$ V in the linear regime are simultaneously shown. For the Schottky-HFETs, we observe a singular behavior of the factor K_{HFET} at $V_G \simeq -5$ V; in the regime below this voltage, the factor K_{HFET} exhibits a weak change. In this regime, the drain current is dominated by the gate leakage as shown in Fig. 9(b). As a result, the LFN is also dominated by the gate leakage, as confirmed by the relation $S_{I_D}f \propto I_G{}^2$ shown in Fig. 9(c). On the other hand, LFN in the MIS-HFETs is always dominated by only the channel current.

For the channel-current-dominated LFN, assuming the HFET on-resistance R_{on} given by the series connection of the intrinsic resistance $R_{int} = r_s\, L_G/W$, where r_s is the sheet resistance of the gated region, and the extrinsic resistance R_{ext} of the ungated part, we also obtain

$$S_{I_D} = S_{I_D}^{int} \frac{R_{int}{}^2}{(R_{int} + R_{ext})^2} + S_{I_D}^{ext} \frac{R_{ext}{}^2}{(R_{int} + R_{ext})^2} \tag{4}$$

and

$$K_{HFET} = \frac{S_{I_D} f}{I_D{}^2} = K_{int} \frac{R_{int}{}^2}{(R_{int} + R_{ext})^2} + K_{ext} \frac{R_{ext}{}^2}{(R_{int} + R_{ext})^2}, \tag{5}$$

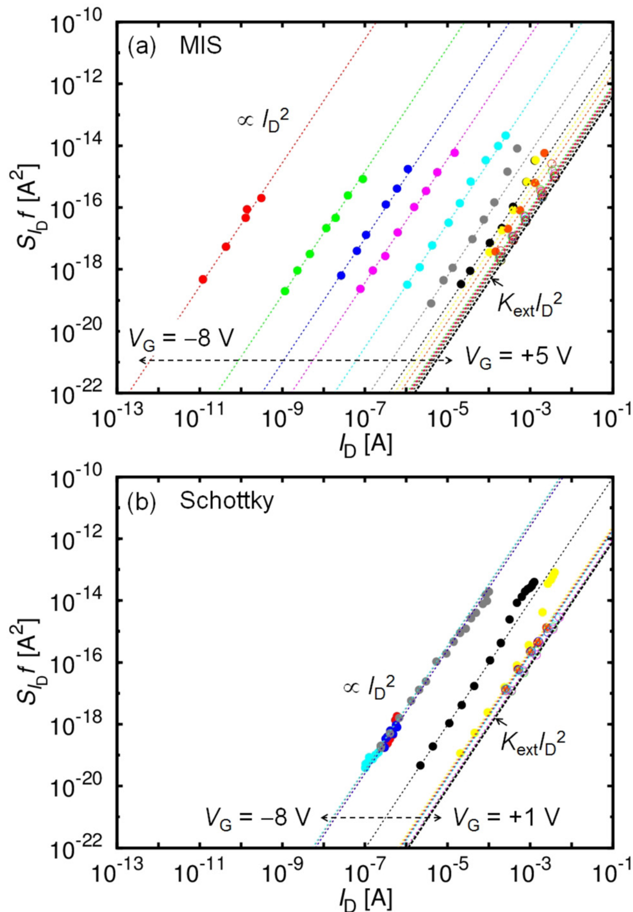

FIG. 8. $S_{I_D}f$ as functions of I_D for (a) MIS- and (b) Schottky-HFETs. The line of $K_{ext}I_D{}^2$ is given.

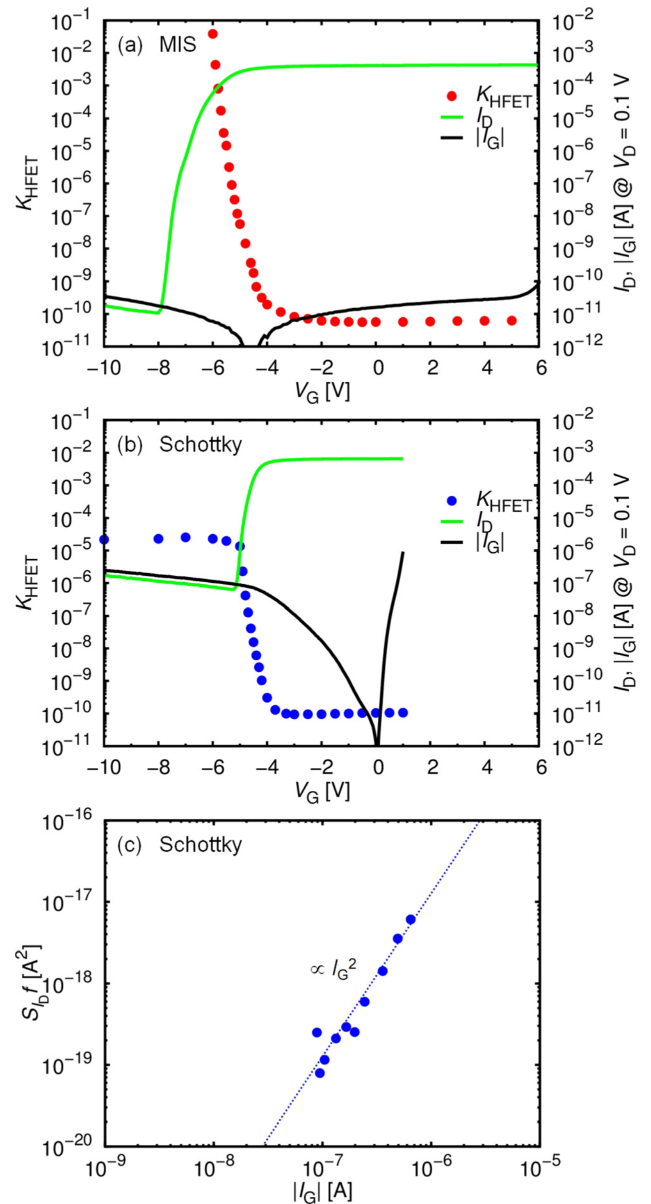

FIG. 9. K_{HFET} as a function of V_G for (a) MIS- and (b) Schottky-HFETs, with I_D and I_G in the linear regime. (c) $S_{I_D}f$ as a function of $|I_G|$ for Schottky-HFETs.

[This article is copyrighted as indicated in the article. Reuse of AIP content is subject to the terms at: http://scitation.aip.org/termsconditions. Downloaded to] IP: 150.65.7.11 On: Mon, 14 Sep 2015 04:02:23

where $S_{I_D}^{int}$ is the PSD generated by the intrinsic gated region with a factor K_{int} depending on V_G, and $S_{I_D}^{ext}$ is that by the extrinsic ungated part with a factor K_{ext} independent of V_G. Since the contribution from the ungated part in Eq. (4) is less than $S_{I_D}^{ext}$, when $S_{I_D} \gg S_{I_D}^{ext} = K_{ext} I_D{}^2/f$, S_{I_D} is dominated by the intrinsic noise. From the value of the R_{ext} obtained by the DC characterization, we can evaluate K_{ext} of the ungated part using the relation given in Fig. 6(b); $K_{ext} \simeq 4.0 \times 10^{-11}$ and 8.2×10^{-11} for the MIS- and Schottky-HFETs, respectively. In Fig. 8, $K_{ext} I_D{}^2$ is shown by the dotted line; data points approach to the line for large V_G. Using the value of K_{ext}, we can evaluate the contributions to the factor K_{HFET} from the first intrinsic and second extrinsic terms in Eq. (5) as shown in Fig. 10, and also obtain K_{int} depending on V_G. In Figs. 11(a) and 11(b), we show the relation between K_{int} and the sheet resistance r_s of the gated region for the MIS- and Schottky-HFETs, respectively. For the small r_s below the middle of $10^3\,\Omega/\text{sq.}$ range, $K_{int} \propto r_s{}^{-2}$ for both the MIS- and Schottky-HFETs. On the other hand, the MIS-HFETs for $r_s \gtrsim 10^5\,\Omega/\text{sq.}$ exhibit $K_{int} \propto r_s{}^2$, while the Schottky-HFETs for $r_s \gtrsim 10^4\,\Omega/\text{sq.}$ exhibit $K_{int} \propto r_s$. The K_{int} is given by

$$K_{int} = \frac{\alpha}{N} = \frac{\alpha}{n_s L_G W}, \qquad (6)$$

where α is the effective Hooge parameter, N is the total electron number, and n_s is the sheet electron concentration in the intrinsic gated region. Therefore, in order to obtain α, it is necessary to evaluate n_s depending on V_G. Measuring *C-V* characteristics of capacitors simultaneously fabricated, we obtain the capacitance C, and n_s calculated from the integration of C,[18–20] as shown in Figs. 12(a) and 12(b), for the MIS and Schottky devices, respectively. As a result, we obtain the Hooge parameter α as a function of n_s shown in Figs. 13(a) and 13(b) for the MIS- and Schottky-HFETs, respectively. We carried out the same analysis for HFETs with a different gate length $L_G = 160\,\text{nm}$, whose results are also given in Fig. 13. The point of α_{ug} for the ungated region is simultaneously plotted in Fig. 13. For the MIS-HFETs with the small $n_s \lesssim 5 \times 10^{11}\,\text{cm}^{-2}$, with increase in n_s, we obtain decrease in $\alpha \propto n_s{}^{-1}$. This behavior of $\alpha \propto n_s{}^{-1}$ is also observed for the Schottky-HFETs for $n_s \lesssim 10^{12}\,\text{cm}^{-2}$. On the other hand, for $5 \times 10^{11}\,\text{cm}^{-2} \lesssim n_s \lesssim 1 \times 10^{12}\,\text{cm}^{-2}$, the MIS-HFETs exhibit rapid decrease in α like $n_s{}^{-\xi}$ with $\xi \sim 2\text{-}3$, which is not observed for the Schottky-HFETs. Moreover, we obtain strong increase in $\alpha \propto n_s{}^3$ for $n_s \gtrsim 2 \times 10^{12}\,\text{cm}^{-2}$ for both the MIS- and Schottky-HFETs.

The regime of $\alpha \propto n_s{}^{-1}$ corresponds to $K_{int} \propto r_s{}^2$ for the MIS-HFETs and $K_{int} \propto r_s$ for the Schottky-HFETs; this difference is caused by different relations between n_s and the electron mobility μ in the intrinsic region. The relation

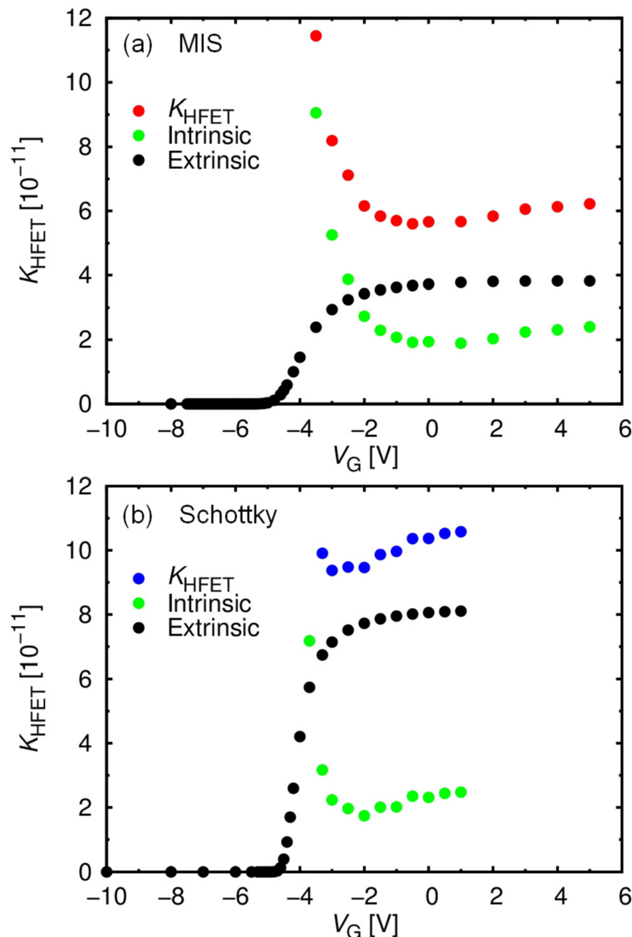

FIG. 10. The intrinsic and extrinsic contributions to K_{HFET} for (a) MIS- and (b) Schottky-HFETs.

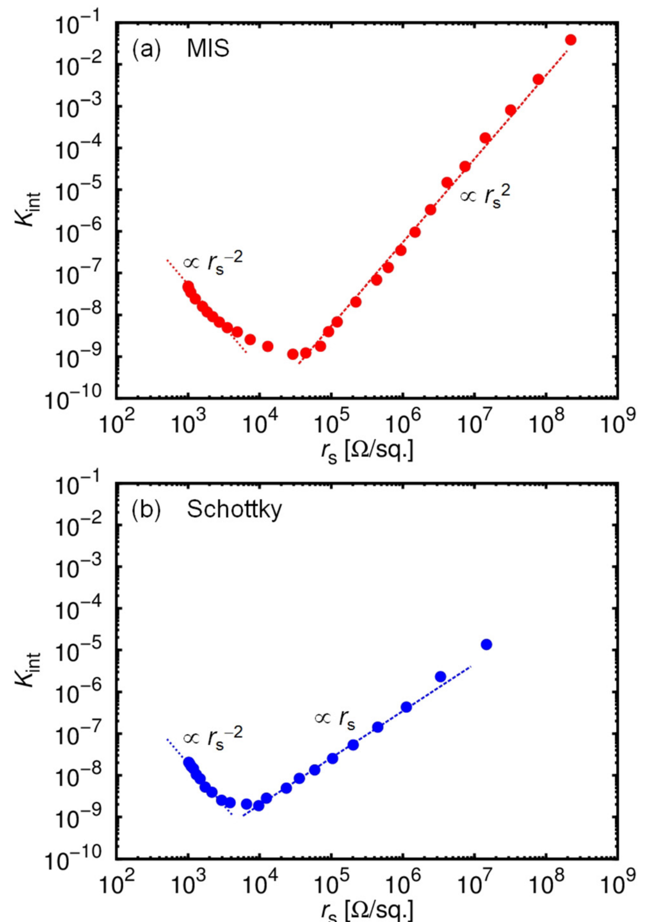

FIG. 11. K_{int} as a function of the sheet resistance r_s of the gated region for (a) MIS- and (b) Schottky-HFETs.

[This article is copyrighted as indicated in the article. Reuse of AIP content is subject to the terms at: http://scitation.aip.org/termsconditions. Downloaded to] IP: 150.65.7.11 On: Mon, 14 Sep 2015 04:02:23

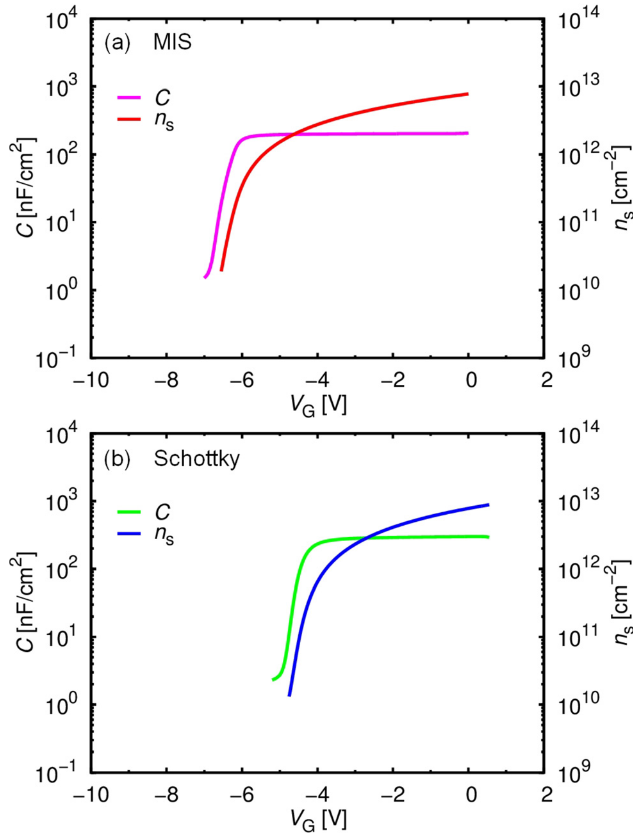

FIG. 12. The capacitance C, and the sheet electron concentration n_s under the gate calculated from the integration of C, as functions of V_G, for (a) MIS and (b) Schottky devices.

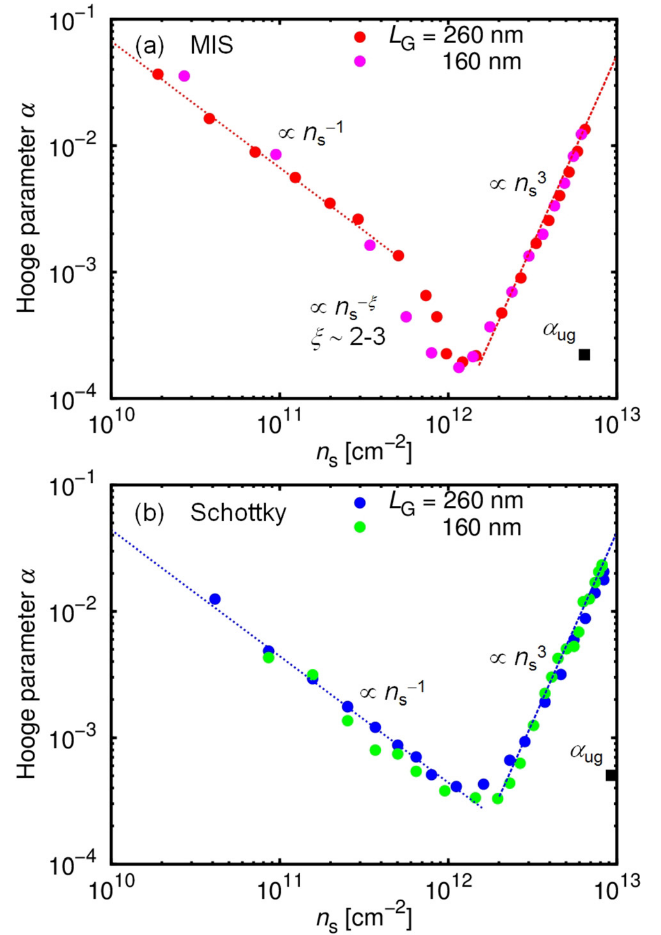

FIG. 13. The Hooge parameter α as a function of the sheet electron concentration n_s under the gate for (a) MIS- and (b) Schottky-HFETs.

$K_{\rm int} \propto r_s \propto (n_s\mu)^{-1}$ for the Schottky-HFETs indicates $\mu \propto n_s$, while $K_{\rm int} \propto {r_s}^2 \propto (n_s\mu)^{-2}$ for the MIS-HFETs does $\mu \simeq$ const. in this regime. This behavior of $\alpha \propto {n_s}^{-1}$ is often observed,[17–20,26,41] and can be attributed to the electron number fluctuation due to electron traps in AlGaN. In general, according to Burgess theorem,[42] we obtain the current fluctuation

$$\frac{(\delta I)^2}{I^2} = \frac{1}{N}\left[\frac{(\delta\mu)^2}{\mu^2} + \frac{(\delta N)^2}{N}\right] \simeq \int_{f_\ell}^{f_h} \frac{S_I}{I^2}\mathrm{d}f \simeq \int_{f_\ell}^{f_h} \frac{\alpha}{Nf}\mathrm{d}f = \frac{\alpha}{N}\ln\frac{f_h}{f_\ell}, \tag{7}$$

where f_ℓ and f_h are the lower and higher limits of the 1/f spectrum, respectively.[43] This gives

$$\alpha \ln\frac{f_h}{f_\ell} \simeq \frac{(\delta\mu)^2}{\mu^2} + \frac{(\delta N)^2}{N}. \tag{8}$$

The first and second terms correspond to the mobility fluctuation and the electron number fluctuation, respectively. If the electron number fluctuation is dominant, the Hooge parameter is given by

$$\alpha \simeq \frac{(\delta N)^2}{N \ln f_h/f_\ell}. \tag{9}$$

Assuming the electron number fluctuation caused by the traps with a density D_0 (in the unit of [cm^{-2} eV^{-1}]), we obtain[44]

$$\alpha \sim \frac{D_0 k_B T}{n_s}, \tag{10}$$

which explains the behavior of $\alpha \propto {n_s}^{-1}$. It is natural to consider that this behavior should be significantly influenced by the AlN/AlGaN interface states in the MIS-HFETs, whose density is rather high, 10^{13} cm^{-2} eV^{-1} order or more for energy levels near the AlGaN conduction band bottom.[7,8] However, the MIS-HFETs and Schottky-HFETs show similar behaviors of $\alpha \simeq 6.8 \times 10^8$ cm^{-2} $\times {n_s}^{-1}$ and $\alpha \simeq 4.4 \times 10^8$ cm^{-2} $\times {n_s}^{-1}$, respectively, both giving D_0 of 10^{11} cm^{-2} eV^{-1} order. In this gate bias regime, AlN/AlGaN interface state energy levels corresponding to the Fermi energy are deep and have extremely long trapping time constants, for example, calculated to be $\sim 5 \times 10^3$ s for 0.7 eV below the AlGaN conduction band bottom.[8] As a result, trapped electrons at the AlN/AlGaN interface states almost "freeze" and, consequently, hardly contribute to the electron number fluctuation. We consider that, for both the MIS- and Schottky-HFETs, the observed $D_0 \sim 10^{11}$ cm^{-2}eV^{-1} is reasonable for traps in AlGaN close to the AlGaN/GaN interface, which have much shorter time constants. On the other hand, the rapid decrease in α like ${n_s}^{-\xi}$ with $\xi \sim$ 2-3 is observed only for the MIS-HFET. We tentatively assume that this behavior is attributed to the mobility fluctuation specific for the MIS-HFETs. In addition, for both the MIS- and

[This article is copyrighted as indicated in the article. Reuse of AIP content is subject to the terms at: http://scitation.aip.org/termsconditions. Downloaded to] IP: 150.65.7.11 On: Mon, 14 Sep 2015 04:02:23

Schottky-HFETs, we observe the strong increase in $\alpha \propto n_s{}^3$ for large n_s. This corresponds to $K_{int} \propto r_s{}^{-2}$, indicating $\mu \simeq$ const. Such increase was observed for Schottky-HFETs with large V_G (Refs. 18–20) and sometimes attributed to large gate leakage currents. However, this behavior cannot be attributed to the gate leakage, which is significantly suppressed in the MIS-HFETs, but can be related to the fluctuation in the intrinsic gate voltage, which is enhanced for large V_G and n_s by the fluctuation of the voltage across the extrinsic source resistance. According to this, α of the gated region is larger than α_{ug} of the ungated region for the same sheet electron concentration, as confirmed in Fig. 13. Even for the intrinsic gated region, the LFN can be influenced by the extrinsic part through the fluctuation of the intrinsic gate voltage.

V. CONCLUSION

We have systematically investigated LFN in AlN/AlGaN/GaN MIS devices in comparison with that in AlGaN/GaN Schottky devices. By measuring LFN in ungated two-terminal devices and HFETs, we elucidated LFN characteristics in the intrinsic gated region of the HFETs. Although there is a bias regime of the Schottky HFETs in which LFN is dominated by the gate leakage current, LFN in the MIS-HFETs is always dominated by only the channel current. Analyzing the channel-current-dominated LFN, we obtained Hooge parameters for the gated region as a function of the sheet electron concentration under the gate, which exhibits different behaviors for the MIS- and Schottky-HFETs.

[1]T. Hashizume, S. Ootomo, and H. Hasegawa, Appl. Phys. Lett. **83**, 2952 (2003).
[2]C. Liu, E. F. Chor, and L. S. Tan, Appl. Phys. Lett. **88**, 173504 (2006).
[3]A. Kawano, S. Kishimoto, Y. Ohno, K. Maezawa, T. Mizutani, H. Ueno, T. Ueda, and T. Tanaka, Phys. Status Solidi C **4**, 2700 (2007).
[4]Y.-L. Chiou, C.-S. Lee, and C.-T. Lee, Appl. Phys. Lett. **97**, 032107 (2010).
[5]Y. Liu, J. A. Bardwell, S. P. McAlister, S. Rolfe, H. Tang, and J. B. Webb, Phys. Status Solidi C **0**, 69 (2002).
[6]R. Stoklas, D. Gregušová, Š. Gaži, J. Novák, and P. Kordoš, J. Vac. Sci. Technol. B **29**, 01A809 (2011).
[7]H.-A. Shih, M. Kudo, M. Akabori, and T. Suzuki, Jpn. J. Appl. Phys., Part 1 **51**, 02BF01 (2012).
[8]H.-A. Shih, M. Kudo, and T. Suzuki, Appl. Phys. Lett. **101**, 043501 (2012).
[9]J.-C. Gerbedoen, A. Soltani, M. Mattalah, M. Moreau, P. Thevenin, and J.-C. D. Jaeger, Diamond Relat. Mater. **18**, 1039 (2009).
[10]T. Q. Nguyen, H.-A. Shih, M. Kudo, and T. Suzuki, Phys. Status Solidi C **10**, 1401 (2013).
[11]M. E. Levinshtein, F. Pascal, S. Contreras, W. Knap, S. L. Rumyantsev, R. Gaska, J. W. Yang, and M. Shur, Appl. Phys. Lett. **72**, 3053 (1998).
[12]M. E. Levinshtein, S. L. Rumyantsev, R. Gaska, J. W. Yang, and M. S. Shur, Appl. Phys. Lett. **73**, 1089 (1998).
[13]D. Kuksenkov, H. Temkin, R. Gaska, and J. Yang, IEEE Electron Device Lett. **19**, 222 (1998).
[14]W. Y. Ho, C. Surya, K. Y. Tong, W. Kim, A. Botcharev, and H. Morkoc, IEEE Trans. Electron Devices **46**, 1099 (1999).
[15]M. E. Levinshtein, S. L. Rumyantsev, D. C. Look, R. J. Molnar, M. A. Khan, G. Simin, V. Adivarahan, and M. S. Shur, J. Appl. Phys. **86**, 5075 (1999).
[16]A. Balandin, S. Morozov, G. Wijeratne, S. J. Cai, R. Li, J. Li, K. L. Wang, C. R. Viswanathan, and Y. Dubrovskii, Appl. Phys. Lett. **75**, 2064 (1999).
[17]J. A. Garrido, B. E. Foutz, J. A. Smart, J. R. Shealy, M. J. Murphy, W. J. Schaff, L. F. Eastman, and E. Muñoz, Appl. Phys. Lett. **76**, 3442 (2000).
[18]S. L. Rumyantsev, N. Pala, M. S. Shur, M. E. Levinshtein, P. A. Ivanov, M. A. Khan, G. Simin, J. Yang, X. Hu, A. Tarakji, and R. Gaska, Fluctuation Noise Lett. **01**, L221 (2001).
[19]S. L. Rumyantsev, N. Pala, M. S. Shur, R. Gaska, M. E. Levinshtein, P. A. Ivanov, M. A. Khan, G. Simin, X. Hu, and J. Yang, Semicond. Sci. Technol. **17**, 476 (2002).
[20]N. Pala, S. Rumyantsev, M. Shur, R. Gaska, X. Hu, J. Yang, G. Simin, and M. Khan, Solid-State Electron. **47**, 1099 (2003).
[21]S. L. Rumyantsev, N. Pala, M. S. Shur, M. E. Levinshtein, M. Asif Khan, G. Simin, and J. Yang, J. Appl. Phys. **93**, 10030 (2003).
[22]S. L. Rumyantsev, M. S. Shur, N. Dyakonova, W. Knap, Y. Meziani, F. Pascal, A. Hoffman, X. Hu, Q. Fareed, Y. Bilenko, and R. Gaska, J. Appl. Phys. **96**, 3845 (2004).
[23]A. P. Dmitriev, M. E. Levinshtein, S. L. Rumyantsev, and M. S. Shur, J. Appl. Phys. **97**, 123706 (2005).
[24]S. A. Vitusevich, S. V. Danylyuk, N. Klein, M. V. Petrychuk, V. N. Sokolov, V. A. Kochelap, A. E. Belyaev, V. Tilak, J. Smart, A. Vertiatchikh, and L. F. Eastman, Appl. Phys. Lett. **80**, 2126 (2002).
[25]A. Vertiatchikh and L. F. Eastman, SEE Electron Device Lett. **24**, 535 (2003).
[26]H. Rao and G. Bosman, J. Appl. Phys. **106**, 103712 (2009).
[27]C. Kayis, C. Y. Zhu, M. Wu, X. Li, U. Ozgur, and H. Morkoc, J. Appl. Phys. **109**, 084522 (2011).
[28]T. Roy, Y. S. Puzyrev, E. X. Zhang, S. DasGupta, S. A. Francis, D. M. Fleetwood, R. D. Schrimpf, U. K. Mishra, J. S. Speck, and S. T. Pantelides, Microelectron. Reliab. **51**, 212 (2011).
[29]H.-C. Chiu, C.-H. Chen, H.-L. Kao, F.-T. Chien, P.-K. Weng, Y.-T. Gau, and H.-W. Chuang, Microelectron. Reliab. **53**, 1897 (2013).
[30]N. Pala, R. Gaska, S. Rumyantsev, M. Shur, M. A. Khan, X. Hu, G. Simin, and J. Yang, Electron. Lett. **36**, 268 (2000).
[31]S. L. Rumyantsev, N. Pala, M. S. Shur, R. Gaska, M. E. Levinshtein, M. A. Khan, G. Simin, X. Hu, and J. Yang, J. Appl. Phys. **88**, 6726 (2000).
[32]S. L. Rumyantsev, N. Pala, M. S. Shur, R. Gaska, M. E. Levinshtein, M. A. Khan, G. Simin, X. Hu, and J. Yang, J. Appl. Phys. **90**, 310 (2001).
[33]P. Valizadeh, D. Pavlidis, K. Shiojima, T. Makimura, and N. Shigekawa, Solid-State Electron. **49**, 1352 (2005).
[34]Y.-Z. Chiou, Y.-K. Su, J. Gong, S.-J. Chang, and C.-K. Wang, Jpn. J. Appl. Phys., Part 1 **45**, 3405 (2006).
[35]L.-H. Huang, S.-H. Yeh, and C.-T. Lee, Appl. Phys. Lett. **93**, 043511 (2008).
[36]C. Kayis, J. H. Leach, C. Zhu, M. Wu, X. Li, U. Özgür, H. Morkoc, X. Yang, V. Misra, and P. Handel, IEEE Electron Device Lett. **31**, 1041 (2010).
[37]C.-T. Lee, Y.-L. Chiou, and C.-S. Lee, IEEE Electron Device Lett. **31**, 1220 (2010).
[38]Y.-L. Chiou and C.-T. Lee, IEEE Trans. Electron Devices **58**, 3869 (2011).
[39]M. Ochiai, M. Akita, Y. Ohno, S. Kishimoto, K. Maezawa, and T. Mizutani, Jpn. J. Appl. Phys., Part 1 **42**, 2278 (2003).
[40]F. N. Hooge, T. G. M. Kleinpenning, and L. K. J. Vandamme, Rep. Prog. Phys. **44**, 479 (1981).
[41]L. K. J. Vandamme, X. Li, and D. Rigaud, IEEE Trans. Electron Devices **41**, 1936 (1994).
[42]R. E. Burgess, J. Phys. Chem. Solids **22**, 371 (1961).
[43]F. N. Hooge, IEEE Trans. Electron Devices **41**, 1926 (1994).
[44]J. Lee, J. Brini, A. Chovet, and C. Dimitriadis, Solid-State Electron. **43**, 2185 (1999).

[This article is copyrighted as indicated in the article. Reuse of AIP content is subject to the terms at: http://scitation.aip.org/termsconditions. Downloaded to] IP: 150.65.7.11 On: Mon, 14 Sep 2015 04:02:23